NASA TECHNICAL NOTE

NASA TN D-5390

NASA TN D-5390

EFFECT OF STRESS RATIO ON FATIGUE-CRACK GROWTH IN 7075-T6 AND 2024-T3 ALUMINUM-ALLOY SPECIMENS

by C. Michael Hudson

Langley Research Center
Langley Station, Hampton, Va.

NATIONAL AERONAUTICS AND SPACE ADMINISTRATION • WASHINGTON, D. C. • AUGUST 1969

1. Report No. NASA TN D-5390	2. Government Accession No.	3. Recipient's Catalog No.
4. Title and Subtitle EFFECT OF STRESS RATIO ON FATIGUE-CRACK GROWTH IN 7075-T6 AND 2024-T3 ALUMINUM-ALLOY SPECIMENS		5. Report Date August 1969 6. Performing Organization Code
7. Author(s) C. Michael Hudson		8. Performing Organization Report No. L-6662
9. Performing Organization Name and Address NASA Langley Research Center Hampton, Va. 23365		10. Work Unit No. 126-14-15-01-23 11. Contract or Grant No. 13. Type of Report and Period Covered Technical Note
12. Sponsoring Agency Name and Address National Aeronautics and Space Administration Washington, D.C. 20546		14. Sponsoring Agency Code
15. Supplementary Notes		

16. Abstract

Axial-load fatigue-crack-growth tests were conducted on 12-inch-wide (305-mm) sheet specimens made of 7075-T6 and 2024-T3 aluminum alloy. These tests were made at stress ratios R (ratio of the minimum stress to the maximum stress) ranging from -1.0 to 0.8 and at maximum stress levels ranging from 5 to 50 ksi (34 to 340 MN/m^2) to study the effects of stress ratio on fatigue-crack growth.

The experimental results were analyzed by using the stress-intensity method. For a given positive stress ratio, the fatigue-crack-growth rate was a single-valued function of the stress-intensity range for both 7075-T6 and 2024-T3 aluminum alloys. For $R \geq 0$ the crack-growth rates varied systematically with R for both materials; the higher stress ratios produced higher rates of fatigue-crack growth for a given stress-intensity range.

Fatigue cracks in the 7075-T6 aluminum alloy grew at the same rates in all tests with $R \leq 0$ when the same maximum stress-intensity factor was applied. In contrast, fatigue cracks in the 2024-T3 aluminum alloy grew faster in the tests with $R = -1$ than in the tests with $R = 0$ when the same maximum stress-intensity factor was applied.

Empirical equations previously developed by various investigators were fitted to the experimental data. In general, good correlation was obtained.

17. Key Words Suggested by Author(s) Fatigue Crack propagation Stress ratio	18. Distribution Statement Unclassified – Unlimited		
19. Security Classif. (of this report) Unclassified	20. Security Classif. (of this page) Unclassified	21. No. of Pages 29	22. Price* $3.00

*For sale by the Clearinghouse for Federal Scientific and Technical Information
Springfield, Virginia 22151

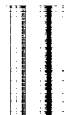

EFFECT OF STRESS RATIO ON FATIGUE-CRACK GROWTH IN 7075-T6 AND 2024-T3 ALUMINUM-ALLOY SPECIMENS

By C. Michael Hudson
Langley Research Center

SUMMARY

Axial-load fatigue-crack-growth tests were conducted on 12-inch-wide (305-mm) sheet specimens made of 7075-T6 and 2024-T3 aluminum alloy. These tests were made at stress ratios R (ratio of the minimum stress to the maximum stress) ranging from -1.0 to 0.8 and at maximum stress levels ranging from 5 to 50 ksi (34 to 340 MN/m^2) to study the effects of stress ratio on fatigue-crack growth.

The experimental results were analyzed by using the stress-intensity method. For a given positive stress ratio, the fatigue-crack-growth rate was a single-valued function of the stress-intensity range for both 7075-T6 and 2024-T3 aluminum alloys. For $R \geq 0$ the crack-growth rates varied systematically with R for both materials; the higher stress ratios produced higher rates of fatigue-crack growth for a given stress-intensity range.

Fatigue cracks in the 7075-T6 aluminum alloy grew at the same rates in all tests with $R \leq 0$ when the same maximum stress-intensity factor was applied. In contrast, fatigue cracks in the 2024-T3 aluminum alloy grew faster in the tests with $R = -1$ than in the tests with $R = 0$ when the same maximum stress-intensity factor was applied.

Empirical equations developed by Forman et al. (in Trans. ASME, Ser. D: J. Basic Eng., vol. 89, no. 3, Sept. 1967), by Erdogan (in NASA CR-901), and by Paris (in book entitled "Fatigue – An Interdisciplinary Approach," Syracuse Univ. Press, 1964) were fitted to the data. Forman's equation produced an excellent fit to both the 7075-T6 and the 2024-T3 data. Erdogan's and Paris' equations showed good correlation with the test data except at the higher growth rates for the 7075-T6 alloy.

INTRODUCTION

Fatigue cracks frequently initiate early in the life of cyclically loaded structural components. Consequently, a major portion of the useful life of these components is spent in the crack-propagation phase of fatigue. Fatigue-crack propagation has been shown to be dependent upon the applied stress-intensity range and upon the stress

ratio R (ratio of the minimum stress to the maximum stress). While much information has been obtained for various stress-intensity ranges, much less information is available with regard to stress ratio. Accordingly, an investigation has been conducted to determine the effects of a wide range of R values and stresses on fatigue-crack growth in 7075-T6 and 2024-T3 aluminum-alloy sheet specimens. These materials were selected because of their frequent use in aircraft construction.

The data were analyzed by using the stress-intensity method. Figge and Newman (ref. 1) showed that by this method the data from simple sheet specimens could be used to predict fatigue-crack-growth behavior in simulated structural configurations. Empirical equations developed by Forman, Kearney, and Engle (ref. 2), by Erdogan (ref. 3), and by Paris (ref. 4) were fitted to the data generated in this investigation by using least-squares techniques.

SYMBOLS

The units used for the physical quantities defined in this paper are given both in U.S. Customary Units and in the International System of Units (SI) (ref. 5). The appendix presents factors relating these two systems of units.

a	one-half of total length of a central symmetrical crack, inches (mm)
a_f	half-length of crack immediately prior to rapid fracture, inches (mm)
a_i	half-length of crack at onset of slow crack growth, inches (mm)
C, C_1, C_2	constants in fatigue-crack-growth equations
k_c	critical stress-intensity factor at failure, psi-$\sqrt{\text{in}}$ $\left(\text{MN}/\text{m}^{3/2}\right)$
k_{max}	stress-intensity factor corresponding to maximum cyclic stress (with tangent-formula width correction), ksi-$\sqrt{\text{in}}$ $\left(\text{MN}/\text{m}^{3/2}\right)$
k_{min}	stress-intensity factor corresponding to minimum cyclic stress (with tangent-formula width correction), ksi-$\sqrt{\text{in}}$ $\left(\text{MN}/\text{m}^{3/2}\right)$
Δk	range of stress-intensity factor (with tangent-formula width correction), $k_{max} - k_{min}$, ksi-$\sqrt{\text{in}}$ $\left(\text{MN}/\text{m}^{3/2}\right)$
m, n, p	exponents in fatigue-crack-growth equations

N	number of cycles
P_a	amplitude of load applied in a cycle, kips (newtons)
P_f	load on specimen immediately prior to rapid fracture, kips (newtons)
P_i	load on specimen at onset of slow crack growth, kips (newtons)
P_m	mean load applied in a cycle, kips (newtons)
P_{max}	maximum load applied in a cycle, kips (newtons)
P_{min}	minimum load applied in a cycle, $P_m - P_a$, kips (newtons)
R	ratio of minimum stress to maximum stress
S_a	alternating stress, P_a/wt, ksi (MN/m^2)
S_m	mean stress, P_m/wt, ksi (MN/m^2)
S_{max}	maximum gross stress, P_{max}/wt, ksi (MN/m^2)
S_{min}	minimum gross stress, P_{min}/wt, ksi (MN/m^2)
t	specimen thickness, inches (mm)
w	specimen width, inches (mm)
x	length of crack starter notch, inches (mm)
α	correction for finite width of panel

SPECIMENS, TESTS, AND PROCEDURES

Specimens

The materials were taken from the special stocks of 7075-T6 and 2024-T3 aluminum-alloy sheets retained at Langley Research Center for fatigue testing. The fatigue properties of these materials are discussed in reference 6. Tensile properties were obtained in this investigation by using standard American Society for Testing and

Materials (ASTM) tensile specimens and are listed in table I. Also listed in table I are the tensile properties obtained in 1949 on the same stocks of material. The tensile properties of the materials did not change significantly over the 19-year interval. The specimen configuration used in the crack propagation and in ancillary residual-static-strength tests is shown in figure 1. Sheet specimens 12 inches (305 mm) wide, 35 inches (889 mm) long, and with a nominal thickness of 0.090 inch (2.28 mm) were tested. A notch 0.10 inch (2.54 mm) long by 0.01 inch (0.25 mm) wide was cut into the center of each specimen by an electrical discharge process. Only very localized heating occurs in making notches in this manner. Thus virtually all of the material through which the fatigue crack propagates is unaltered by the cutting process. All specimens were made with the longitudinal axis of the specimens parallel to the rolling direction of the sheets.

A reference grid (ref. 7) was photographically printed on the surface of the specimens to mark intervals in the path of the crack. Metallographic examination and tensile tests conducted on specimens bearing the grid indicated that the grid had no detrimental effect on the material.

Testing Machines

Four axial-load fatigue-testing machines were employed in this investigation. The capabilities of these machines are listed in the following table:

Machine type	Maximum load capability		Operating frequency		Machine description
	lbf	kN	cpm	Hz	
Subresonant	20 000	89	1800	30	Reference 8
Hydraulic	100 000	445	1200	20	Reference 9
Hydraulic	120 000	534	30	0.5	Reference 10
Combination:					
As subresonant unit . . .	105 000	467	820	14	Reference 11
As hydraulic unit	132 000	587	40 to 60	0.7 to 1.0	

Loads were continuously monitored on these machines by measuring the output of a strain-gage bridge attached to a dynamometer in series with the specimens. The maximum error in loading was ±1 percent of the applied load.

Test Procedure

Axial-load fatigue-crack-propagation tests were conducted at stress ratios R ranging from -1.0 to 0.8 for 7075-T6 aluminum alloy and from -1.0 to 0.7 for 2024-T3 aluminum alloy. Generally, tests were conducted at a number of maximum stress

levels S_{max} for a given stress ratio. The alternating and mean loads were kept constant throughout each test. Duplicate tests were conducted at each stress level.

Fatigue-crack growth was observed through 10-power microscopes while illuminating the specimen with stroboscopic light. The number of cycles required to propagate the crack to each grid line was recorded so that crack-propagation rates could be determined. Approximately two-thirds of the crack-propagation tests were conducted to failure. The remaining one-third were stopped before failure, and the cracked specimens were used in residual-static-strength tests.

In all the tests (crack growth and residual static strength), the specimens were clamped between lubricated guides in order to prevent buckling and out-of-plane vibrations during testing. Light oil was used to lubricate the surfaces of the specimens and the guides. None of this oil was observed to enter the crack during testing. Consequently, the oil was not expected to affect the crack growth. A 0.125-inch (3.2-mm) slot was cut across the width of one guide plate to allow visual observation of the crack.

Axial-load residual-static-strength tests were conducted at a load rate of 120 000 lbf/min (8.9 kN/s) on unfailed crack-propagation specimens. A 70-mm sequence camera operating at 20 frames per second was used to obtain slow-crack-growth data. The cracked section of the specimen and the image of a load-indicating device were photographed on each frame of film by using an optical prism. From this film, the load at which the crack first started to grow statically and the load and crack length immediately prior to final failure were determined.

METHOD OF ANALYSIS

The fatigue-crack-growth data were correlated by the stress-intensity method. It was hypothesized in reference 4 that the rate of fatigue-crack propagation was a function of the stress-intensity range; that is,

$$\frac{da}{dN} = f(\Delta k) \tag{1}$$

where

$$\Delta k = k_{max} - k_{min} \tag{2}$$

For centrally cracked specimens subjected to a uniformly distributed axial load,

$$k_{max} = \alpha S_{max} \sqrt{a} \tag{3}$$

and

$$k_{min} = \alpha S_{min}\sqrt{a} \tag{4}$$

The term α is a factor which corrects for the finite width of the specimen and is given by

$$\alpha = \sqrt{\frac{w}{\pi a} \tan \frac{\pi a}{w}} \tag{5}$$

The term S_{max} is the maximum gross stress in the cycle and S_{min} is the minimum gross stress in the cycle. In presenting the results, the experimental values of da/dN were plotted as functions of Δk (eq. (2)).

RESULTS AND DISCUSSION

Fatigue-Crack Growth

The results of the fatigue-crack-growth tests on 7075-T6 and 2024-T3 specimens are presented in table II. This table gives the average number of cycles required for the crack to grow from a half-length a of 0.10 inch (2.54 mm) to the specified half-lengths. Fatigue-crack-propagation rates da/dN were graphically determined from the crack-growth curves defined in table II.

Typical fatigue-crack-growth curves for 7075-T6 and 2024-T3 specimens tested under identical loading conditions are shown in figure 2. For these identical conditions, two to four times as many cycles were required to reach a given crack length in the 2024-T3 alloy as in the 7075-T6 alloy.

Effect of Stress Ratio

Data for $R \geqq 0$.- The fatigue-crack-growth data from the tests with $R \geqq 0$ are presented in figure 3 as plots of rate as a function of the stress-intensity range Δk. For a given positive stress ratio, rate was a single-valued function of Δk for both 7075-T6 and 2024-T3 alloys. Crack-growth rates varied systematically with R for both materials; the higher stress ratios produced higher rates of fatigue-crack growth for a given value of Δk.

Data for $R \leqq 0$.- The crack-growth rate in the 7075-T6 alloy was a single-valued function of Δk for all negative stress ratios when the compressive portion of the loading cycle was neglected in calculating Δk (fig. 4). That is, for $R < 0$, Δk in equation (2) became k_{max}. These data for negative R fell into the same scatter band as the data for $R = 0$ (for which Δk also equals k_{max}), indicating the compressive

portion of the loading cycle did not significantly affect fatigue-crack growth in 7075-T6 alloy.

The crack-growth rate in the 2024-T3 alloy was nominally a single-valued function of Δk for the negative stress ratios (e.g., see fig. 5). (Rates do appear to be slightly higher in the low-frequency tests than in the high-frequency ones for this set of data.) However, fatigue cracks in the 2024-T3 alloy grew faster in the tests with $R = -1$ than in the tests with $R = 0$ (see fig. 6). Here again, $\Delta k = k_{max}$ for both the $R = 0$ and $R = -1$ data. These higher rates in the $R = -1$ tests for the same tensile stress-intensity range indicate that the compression portion of the loading cycle accelerated crack growth in the 2024-T3 alloy.

Illg and McEvily (ref. 12) reported similar findings for 7075-T6 and 2024-T3 specimens tested at $R = 0$ and $R = -1$. They proposed that cracks in the 7075-T6 alloy closed completely at zero load and that the material behaved as though no crack existed under compressive loading. Thus, the compressive portion of the loading cycle in the tests with $R < 0$ would do virtually no damage to the material at the tip of a crack, and the crack would propagate as though it were experiencing an $R = 0$ loading only. Illg and McEvily (ref. 12) further observed that cracks in 2024-T3 alloy do not close completely when zero load is reached in the tests with $R = -1$ because of plastic deformation at the crack tip. Thus, the compressive loading in the tests with $R = -1$ would tend to close the cracks and, in doing so, would do additional fatigue damage to the material immediately ahead of the crack tip. This additional damage could be manifest as the higher fatigue-crack-growth rates observed in this investigation.

Correlation of Data With Fatigue-Crack-Growth Equations

Empirical fatigue-crack-growth equations developed by Forman, Kearney, and Engle (ref. 2), by Erdogan (ref. 3), and by Paris (ref. 4) were fitted to the test data. Least-squares techniques were used to determine the appropriate constants for these three equations. (It should be noted that the constants given in this report for these equations are for U.S. Customary Units.) In fitting these equations, all the data from the $R < 0$ tests for 7075-T6 alloy were assumed to apply to the $R = 0$ tests since all the data for $R \leq 0$ fell into the same scatter band. The data for 2024-T3 alloy with $R = -1$ were not used in fitting the equations since there was no method of calculating the effective stress-intensity factor for a crack which is open for an indefinable portion of the compressive loading.

Forman's equation (ref. 2), relating da/dN, Δk, R, and k_c (the critical stress-intensity factor at failure), produced an excellent fit to both the 7075-T6 and the 2024-T3 data (fig. 7). This equation has the form

$$\frac{da}{dN} = \frac{C(\Delta k)^n}{(1 - R)k_c - \Delta k} \tag{6}$$

where C and n are empirically determined constants. The values of k_c for 7075-T6 and 2024-T3 alloys were obtained from the auxiliary residual-static-strength tests. This factor is related to the load at rapid fracture P_f, the associated crack length a_f, and the width-correction factor α, as follows:

$$k_c = \alpha\left(P_f/wt\right)\sqrt{a_f} \tag{7}$$

Average values of k_c of 40 400 psi-in$^{1/2}$ $\left(44.4\ MN/m^{3/2}\right)$ for the 7075-T6 alloy and of 56 600 psi-in$^{1/2}$ $\left(62.2\ MN/m^{3/2}\right)$ for the 2024-T3 alloy were found in these tests (table III). The constants C and n in equation (6) were determined to have the following values:

Material	C	n
7075-T6	2.13×10^{-13}	3.21
2024-T3	3.22×10^{-14}	3.38

The equation developed by Erdogan (ref. 3) was also fitted to the test data (see fig. 8). This equation has the form

$$\frac{da}{dN} = C_1 k_{max}^m \Delta k^p \tag{8}$$

where C_1, m, and p are empirically determined constants. In fitting equation (8) to the test data, these constants were determined to have the following values:

Material	C_1	m	p
7075-T6	1.00×10^{-19}	1.33	2.37
2024-T3	1.04×10^{-19}	1.15	2.44

The curves computed by equation (8) are shown in figure 8. This equation showed good correlation with the test data except at the higher growth rates for the 7075-T6 alloy.

Paris (ref. 4) proposed the following relationship between the rate of fatigue-crack growth and the stress-intensity range (in the notation of the present paper):

$$\frac{da}{dN} = C_2(\Delta k)^4 \tag{9}$$

In equation (9) C_2 is a constant which is proposed to incorporate the effects of material, mean load, loading frequency, and environment. This equation also showed good correlation with the test data except at the higher growth rates for the 7075-T6 alloy (see fig. 9). Separate values of the coefficient C_2 had to be computed for each value of R since R is not a function in equation (9). These coefficients are listed in the following table:

Material	R	C_2
7075-T6	0	5.52×10^{-21}
	.2	6.44
	.33	1.00×10^{-20}
	.5	1.80
	.7	3.95
	.8	6.84
2024-T3	0	2.14×10^{-21}
	.33	5.40
	.5	7.75
	.7	1.24×10^{-20}

The 7075-T6 data in figures 7 to 9 fell into an "S" shape or reflex type of curvature. A reflex curvature is also obtained from Forman's equation; it is induced by Δk approaching $(1 - R)k_c$ in the denominator of equation (6). This intrinsic shape is the primary reason for the excellent fit to the 7075-T6 data obtained by using Forman's equation. The data for the 2024-T3 alloy would probably have had a reflex curvature had tests been conducted at sufficiently high stress-intensity ranges (such that Δk approached $(1 - R)k_c$). A separate investigation of crack-growth behavior at very high rates is currently being conducted.

Erdogan's and Paris' equations do not provide for this reflex curvature. Consequently, these equations cannot fit the 7075-T6 data at the high growth rates as well as Forman's equation did (see figs. 7 to 9) and probably would not fit the 2024-T3 data as well as Forman's equation if there were additional data from tests at high stress-intensity ranges.

CONCLUSIONS

Axial-load fatigue-crack-propagation tests were conducted on sheet specimens 12 inches (305 mm) wide and nominally 0.090 inch (2.28 mm) thick made of 7075-T6 and 2024-T3 aluminum alloys. These tests were at stress ratios R (ratio of the minimum stress to the maximum stress) ranging from -1.0 to 0.8 and at maximum stresses

ranging from 5 to 50 ksi $(34 \text{ to } 340 \text{ MN/m}^2)$ to study the effect of R on fatigue-crack growth. The test results were analyzed by using the stress-intensity method and were correlated with three empirical relations. The following conclusions can be drawn from this study:

1. For a given positive stress ratio, rate was a single-valued function of stress-intensity range for both 7075-T6 and 2024-T3 alloys.

2. For $R \geqq 0$ fatigue-crack-growth rates varied systematically with R for both materials. The higher stress ratios produced higher rates of fatigue-crack growth for a given stress-intensity range.

3. Fatigue cracks in 7075-T6 alloy grew at the same rates in all tests with $R \leqq 0$ when the same maximum stress-intensity factor was applied. These equal rates indicate that the compressive portion of the loading cycle did not significantly affect crack growth in this material.

4. The fatigue cracks in 2024-T3 alloy grew faster in the tests with $R = -1$ than in the tests with $R = 0$ when the same maximum stress-intensity factor was applied. Apparently, the compression portion of the loading cycle accelerated crack growth in this material.

5. For identical loading conditions, two to four times as many cycles were required to reach a given crack length in 2024-T3 alloy as in 7075-T6 alloy.

6. Empirical equations developed by Forman et al. (in Trans. ASME, Ser. D: J. Basic Eng., vol. 89, no. 3, Sept. 1967), by Erdogan (in NASA CR-901), and by Paris (in book entitled "Fatigue – An Interdisciplinary Approach," Syracuse Univ. Press, 1964) were fitted to the data. Forman's equation produced an excellent fit to both the 7075-T6 and the 2024-T3 data. Erdogan's and Paris' equations showed good correlation with the test data except at the higher growth rates for the 7075-T6 alloy.

Langley Research Center,
National Aeronautics and Space Administration,
Langley Station, Hampton, Va., May 29, 1969,
126-14-15-01-23.

APPENDIX

CONVERSION OF U.S. CUSTOMARY UNITS TO SI UNITS

The International System of Units (SI) was adopted by the Eleventh General Conference of Weights and Measures, Paris, October 1960, in Resolution No. 12 (ref. 5). Conversion factors for the units used herein are given in the following table:

To convert from U.S. Customary Units	Multiply by –	To obtain SI units
lbf	4.448222	newtons (N)
in.	2.54×10^{-2}	meters (m)
ksi	6.894757×10^{6}	newtons/meter^2 (N/m^2)
cpm	1.67×10^{-2}	hertz (Hz)

Prefixes and symbols to indicate multiples of units are as follows:

Multiple	Prefix	Symbol
10^{-9}	nano	n
10^{-3}	milli	m
10^{3}	kilo	k
10^{6}	mega	M
10^{9}	giga	G

REFERENCES

1. Figge, I. E.; and Newman, J. C., Jr.: Fatigue Crack Propagation in Structures With Simulated Rivet Forces. Spe. Tech. Publ. No. 415, Amer. Soc. Testing Mater., c.1967, pp. 71-94.

2. Forman, R. G.; Kearney, V. E.; and Engle, R. M.: Numerical Analysis of Crack Propagation in Cyclic-Loaded Structures. Trans. ASME, Ser. D: J. Basic Eng., vol. 89, no. 3, Sept. 1967, pp. 459-464.

3. Erdogan, Fazil: Crack Propagation Theories. NASA CR-901, 1967.

4. Paris, Paul C.: The Fracture Mechanics Approach to Fatigue. Fatigue – An Interdisciplinary Approach, John J. Burke, Norman L. Reed, and Volker Weiss, eds., Syracuse Univ. Press, 1964, pp. 107-132.

5. Comm. on Metric Pract.: ASTM Metric Practice Guide. NBS Handbook 102, U.S. Dep. Com., Mar. 10, 1967.

6. Grover, H. J.; Bishop, S. M.; and Jackson, L. R.: Fatigue Strengths of Aircraft Materials. Axial-Load Fatigue Tests on Unnotched Sheet Specimens of 24S-T3 and 75S-T6 Aluminum Alloys and of SAE 4130 Steel. NACA TN 2324, 1951.

7. Hudson, C. Michael: Fatigue-Crack Propagation in Several Titanium and Stainless-Steel Alloys and One Superalloy. NASA TN D-2331, 1964.

8. Grover, H. J.; Hyler, W. S.; Kuhn, Paul; Landers, Charles B.; and Howell, F. M.: Axial-Load Fatigue Properties of 24S-T and 75S-T Aluminum Alloy as Determined in Several Laboratories. NACA Rep. 1190, 1954. (Supersedes NACA TN 2928.)

9. McEvily, Arthur J., Jr.; and Illg, Walter: The Rate of Fatigue-Crack Propagation in Two Aluminum Alloys. NACA TN 4394, 1958.

10. Illg, Walter: Fatigue Tests on Notched and Unnotched Sheet Specimens of 2024-T3 and 7075-T6 Aluminum Alloys and of SAE 4130 Steel With Special Consideration of the Life Range From 2 to 10,000 Cycles. NACA TN 3866, 1956.

11. Hudson, C. Michael; and Hardrath, Herbert F.: Investigation of the Effects of Variable-Amplitude Loadings on Fatigue Crack Propagation Patterns. NASA TN D-1803, 1963.

12. Illg, Walter; and McEvily, Arthur J., Jr.: The Rate of Fatigue-Crack Propagation for Two Aluminum Alloys Under Completely Reversed Loading. NASA TN D-52, 1959.

TABLE I.- AVERAGE TENSILE PROPERTIES OF MATERIALS TESTED

Material	Ultimate tensile strength		Yield stress (0.2-percent offset)		Young's modulus of elasticity		Elongation in 2-inch (51-mm) gage length, percent	No. of tests
	ksi	MN/m^2	ksi	MN/m^2	ksi	GN/m^2		
1968 data								
7075-T6	83.2	574	75.9	523	10 100	69.6	12	20
2024-T3	70.9	489	51.2	353	10 420	71.8	21	20
1949 data								
7075-T6	82.9	572	75.5	518	10 220	70.5	12	152
2024-T3	72.1	497	52.1	359	10 470	72.2	21	147

TABLE II.- AVERAGE NUMBER OF CYCLES REQUIRED TO EXTEND CRACKS FROM A HALF-LENGTH OF 0.10 INCH (2.54 mm)

(a) 7075-T6 aluminum alloy

S_m		S_a		Loading frequency		Nominal R value	Average number of cycles required to propagate a crack from a half-length a of 0.10 in. (2.54 mm) to a half-length a of –												
ksi	MN/m^2	ksi	MN/m^2	cpm	Hz		0.20 in. (5.08 mm)	0.30 in. (7.62 mm)	0.40 in. (10.16 mm)	0.50 in. (12.70 mm)	0.60 in. (15.24 mm)	0.70 in. (17.78 mm)	0.80 in. (20.32 mm)	0.90 in. (22.86 mm)	1.00 in. (25.40 mm)	1.20 in. (30.48 mm)	1.40 in. (35.56 mm)	1.60 in. (40.64 mm)	1.80 in. (45.72 mm)	2.00 in. (50.80 mm)	2.40 in. (60.96 mm)
0	0	30	207	30	0.5	-1	1 240	1 640	1 865	1 980	2 040	2 080	2 110	2 120	2 140						
0	0	25	172	30	.5	-1	3 230	4 200	4 600	4 860	5 000	5 100	5 160	5 200	5 270	5 330	5 370				
0	0	20	138	820	13.7	-1	4 820	7 170	8 450	9 180	9 600	9 900	10 060	10 200	10 250						
0	0	15	103	1200	20.0	-1	8 000	12 500	15 300	17 300	18 830	19 900	20 700	21 300	21 830	22 700	23 300				
0	0	10	69	1800	30.0	-1	30 000	43 800	52 000	58 100	63 400	67 300	71 000	74 000	76 800	81 100	84 000	86 000			
0	0	5	34	1800	30.0	-1	492 000	770 000	867 000	920 000	960 000	985 000	1 007 000	1 020 000	1 040 000	1 065 000	1 083 000	1 098 000	1 110 000	1 120 000	1 138 000
2.5	17	20	138	820	13.7	-.8	2 500	3 730	4 380	4 760	5 000	5 150	5 280	5 370	5 440						
2.5	17	17.5	121	820	13.7	-.8	5 720	8 700	10 080	10 860	11 370	11 700	11 920	12 120	12 260	12 440					
5	34	25	172	[a]30; 820	0.5; 13.7	-.7	1 375	1 900	2 160	2 320	2 410	2 475	2 525	2 570	2 600	2 640	2 660				
2.5	17	15	103	820	13.7	-.7	5 900	8 500	10 200	11 300	12 130	12 700	13 200	13 500	13 780	14 100	14 360				
2.5	17	12.5	86	1800	30.0	-.7	11 400	16 800	20 100	22 200	23 800	24 800	25 600	26 200	26 700	27 400	27 700				
5	34	20	138	[a]30; 820	0.5; 13.7	-.6	2 640	3 740	4 300	4 640	4 850	5 000	5 100	5 170	5 230	5 270					
2.5	17	10	69	820	13.7	-.6	16 600	24 200	28 500	31 700	34 000	35 800	37 400	38 700	39 900	41 400	42 500	43 100	43 600		
5	34	15	103	820	13.7	-.5	5 300	7 900	9 730	10 680	11 200	11 550	11 800	11 970	12 060	12 200					
10	69	20	138	[a]30; 820	0.5; 13.7	-.33	1 550	2 100	2 350	2 470	2 540	2 580	2 600	2 630	2 633						
5	34	10	69	1800	30.0	-.33	12 300	18 300	22 000	24 500	26 600	28 200	29 300	30 200							
2.5	17	5	34	820	13.7	-.33	140 000	186 000	209 000	223 000	233 000	241 000	248 000	252 000	257 000	264 000	270 000	273 000	276 000		
20	138	30	207	30	0.5	-.2	226	294	316	322	324										
10	69	15	103	[a]30; 820	0.5; 13.7	-.2	2 900	4 300	4 930	5 300	5 540	5 700	5 800	5 900	5 990	6 100	6 160	6 180			
15	103	20	138	30	0.5	-.14	1 060	1 380	1 545	1 630	1 680	1 710	1 730								
25	172	25	172	30	0.5	0	330	413													
20	138	20	138	30	0.5	0	700	930	1 030	1 075	1 100	1 110									
15	103	15	103	[a]30; 820	0.5; 13.7	0	1 670	2 360	2 660	2 820	2 930	3 000	3 050								
10	69	10	69	1200	20.0	0	6 140	8 800	10 370	11 300	11 800	12 300	12 570	12 800	12 950	13 150					
5	34	5	34	1800	30.0	0	70 000	88 300	98 300	105 000	110 000	113 000	117 000	120 000	122 000	127 000	129 000	131 000	132 000		
30	207	20	138	15	0.25	.2	410	490													
25	172	16.7	115	30	0.5	.2	760	990	1 100	1 150	1 180										
20	138	13.3	92	30	0.5	.2	1 680	2 340	2 640	2 830	2 960	3 060	3 120								
15	103	10	69	30	0.5	.2	3 800	5 650	6 550	7 150	7 500	7 750	7 950	8 080	8 190	8 340	8 420				
30	207	15	103	[a]30; 820	0.5; 13.7	.33	810	1 050	1 130	1 170											
25	172	12.5	86	30	0.5	.33	1 500	2 060	2 320	2 470	2 570	2 630	2 680								
20	138	10	69	[a]30; 820	0.5; 13.7	.33	3 040	4 260	4 900	5 280	5 550	5 720	5 850	5 940							
15	103	7.5	52	820	13.7	.33	7 350	10 100	11 700	12 800											
10	69	5	34	1800	30.0	.33	16 100	23 700	28 900	32 600	35 500	37 800	39 500	40 800	42 000	43 500	44 500				
30	207	10	69	[a]30; 820	0.5; 13.7	.5	2 230	3 040	3 430	3 660	3 810	3 920	3 990								
25	172	8.3	57	30	0.5	.5	4 100	5 600	6 380	6 800	7 100	7 260	7 380	7 480	7 500						
20	138	6.7	46	820	13.7	.5	9 500	12 400	13 820	14 730	15 400										
15	103	5	34	820	13.7	.5	18 500	28 000	32 800	35 600	37 600	39 000	40 000	40 800	41 400	42 000	42 500				
10	69	3	21	1800	30.0	.5	105 000	140 000	160 000	175 000	185 000	192 500	197 500	202 500	205 000	212 000	215 000	217 500			
30	207	5	34	820	13.7	.7	12 300	16 300	18 300	19 400	20 200	20 700	21 000								
25	172	4.4	30	820	13.7	.7	19 800	27 000	30 900	33 000	34 200	35 200	36 000	36 500							
20	138	3	21	820	13.7	.7	69 000	97 000	112 000	121 000	127 000	130 000	134 000	136 000	138 000	141 000	143 000	144 000			
15	103	3	21	820	13.7	.7	74 000	98 000	115 000	125 000	132 000	137 000	141 000	144 000	147 000	150 000	152 000	153 000	154 000		
10	69	1.7	12	820	13.7	.7	780 000	1 260 000	1 540 000	1 690 000	1 780 000	1 825 000	1 850 000	1 870 000	1 885 000	1 915 000	1 930 000	1 935 000			
30	207	3	21	820	13.7	.8	42 500	58 750	68 750	75 000	77 500	80 000	82 000	83 750	84 000	85 000					
25	172	2.8	19	820	13.7	.8	71 000	94 000	106 000	111 000	116 000	120 000	122 000	123 000	124 000	126 000					

[a]Duplicate tests at different loading frequencies.

TABLE II.- AVERAGE NUMBER OF CYCLES REQUIRED TO EXTEND CRACKS FROM A HALF-LENGTH OF 0.10 INCH (2.54 mm) – Concluded

(b) 2024-T3 alloy

S_m		S_a		Loading frequency		Nominal R value	Average number of cycles required to propagate a crack from a half-length a of 0.10 in.[a] (2.54 mm) to a half-length a of –												
ksi	MN/m^2	ksi	MN/m^2	cpm	Hz		0.20 in. (5.08 mm)	0.30 in. (7.62 mm)	0.40 in. (10.16 mm)	0.50 in. (12.70 mm)	0.60 in. (15.24 mm)	0.70 in. (17.78 mm)	0.80 in. (20.32 mm)	0.90 in. (22.86 mm)	1.00 in. (25.40 mm)	1.20 in. (30.48 mm)	1.40 in. (35.56 mm)	1.60 in. (40.64 mm)	1.80 in. (45.72 mm)
0	0	25	172	30	0.5	-1	2 340	3 300	3 700	3 950	4 100	4 200	4 280	4 330	4 370				
0	0	20	138	30	0.5	-1	4 850	6 900	8 100	8 900	9 400	9 750	10 000	10 150	10 300				
0	0	15	103	820	13.7	-1	17 700	26 500	32 000	35 800									
0	0	10	69	820	13.7	-1	60 000	89 000	105 000	117 000	127 000	136 000	143 000	148 000	153 000				
0	0	[b]7.5	52	820	13.7	-1		90 000	140 000	170 000	195 000	210 000	225 000	240 000	250 000	265 000	280 000		
15	103	15	103	20	0.3	0	2 800	3 900	4 400	4 700	4 850	5 000							
10	69	10	69	1200	20.0	0	9 000	15 300	19 500	22 000	23 500	24 300	25 000	25 300					
7.5	52	7.5	52	1200	20.0	0	24 000	37 500	46 500	53 000	58 500	62 500	65 500	67 500	69 000	71 500			
5	34	5	34	1200	20.0	0	142 000	178 000	200 000	216 000	228 000	239 000	248 000	256 000	262 000	274 000	282 000	288 000	
3.75	26	3.75	26	1800	30.0	0	610 000	780 000	840 000	880 000	910 000	930 000	950 000	970 000	980 000	1 010 000	1 030 000		
20	138	10	69	1200	20.0	.33	6 100	8 800	10 200	10 900									
15	103	7.5	52	1200	20.0	.33	12 000	18 300	22 700	25 500	27 500	28 800	29 800	30 500	31 100				
12.5	86	6.3	43	1200	20.0	.33	20 500	31 500	39 000	44 000	47 000	50 000	52 000	53 500	55 000				
10	69	5	34	1200	20.0	.33	60 000	82 000	95 000	101 700	115 000	120 000	125 000	130 000	132 000	137 000	140 000	142 000	
5	34	2.5	17	1800	30.0	.33	550 000	780 000	900 000	1 000 000	1 050 000	1 090 000	1 120 000	1 150 000	1 170 000	1 220 000	1 240 000	1 260 000	1 270 000
22.5	155	7.5	52	1200	20.0	.5	9 500	14 000	16 500	18 000	18 800	19 200							
18.75	129	6.25	43	1200	20.0	.5	18 500	27 500	32 500	35 600	38 200	40 000	41 000	42 100	42 600				
15	103	5	34	1200	20.0	.5	29 000	43 000	51 000	57 000	62 000	66 000	69 000	71 000	73 000	75 000	76 000		
11.25	78	3.75	26	1200	20.0	.5	165 000	213 000	238 000	255 000	270 000	280 000	289 000	298 000	303 000	312 000	318 000		
7.5	52	2.5	17	1800	30.0	.5	1 100 000	1 670 000	1 870 000	1 930 000	1 980 000	2 020 000	2 050 000	2 080 000	2 100 000	2 130 000	2 160 000		
30	207	5	34	820	13.7	.7	51 000	67 000	73 000	77 000									
25	172	4.4	30	820	13.7	.7	84 000	107 000	119 000	126 000									
20	138	3.5	24	820	13.7	.7	248 000	296 000	322 000	338 000	350 000	359 000	366 000	370 000					
15	103	2.6	18	820	13.7	.7	590 000	810 000	890 000	940 000	970 000	1 000 000	1 020 000	1 040 000	1 050 000	1 070 000			
10	69	[c]1.7	12	820	13.7	.7			1 000 000	1 500 000	1 750 000	1 890 000	2 000 000	2 070 000	2 150 000	2 210 000	2 250 000		

[a]Except as noted.

[b]Crack was initiated and propagated to a = 0.15 inch (3.8 mm) at S_a = 10 ksi (69 MN/m^2) to expedite testing; cycles listed are number required to propagate crack from a = 0.20 inch (5.08 mm).

[c]Crack was initiated and propagated to a = 0.18 inch (4.6 mm) at S_a = 5 ksi (34 MN/m^2) to expedite testing; cycles listed are number required to propagate crack from a = 0.30 inch (7.62 mm).

TABLE III.- CRACK AND LOAD MEASUREMENTS AND VALUES OF k_c FROM RESIDUAL-STATIC-STRENGTH TESTS

(a) 7075-T6 alloy

a_i		a_f		P_i		P_f		k_c	
in.	mm	in.	mm	kips	kN	kips	kN	ksi-in$^{1/2}$	MN/m$^{3/2}$
1.72	43.69	1.85	46.99	23.4	104	29.9	133	39.2	43.1
1.59	40.39	1.80	45.72	17.7	79	30.4	135	39.2	43.1
1.53	38.86	1.79	45.43	20.0	89	30.4	135	38.5	42.3
1.94	49.28	2.36	59.95	16.5	73	27.2	121	39.8	43.7
1.02	25.91	1.16	29.46	----	---	38.5	171	38.0	41.7
.98	24.89	1.19	30.22	----	---	38.8	173	39.7	43.7
.91	23.11	.96	24.38	----	---	43.1	192	38.0	41.7
1.01	25.65	1.09	27.69	----	---	41.7	185	41.4	45.5
1.05	26.67	1.15	29.21	29.2	130	37.7	168	38.4	42.2
.78	19.81	.94	23.88	32.8	146	44.5	198	41.6	45.7
1.31	33.27	1.75	44.45	19.2	85	32.0	142	40.2	44.2
1.90	48.26	2.19	55.63	15.7	70	25.0	111	35.4	39.0
.52	13.21	.73	18.54	32.8	146	50.4	224	40.4	44.4
1.22	30.99	1.53	38.86	25.8	115	35.9	160	42.0	46.2
1.76	44.70	2.10	53.34	18.3	81	30.2	134	41.8	45.9
1.40	35.56	1.73	43.94	26.8	119	32.3	144	41.0	45.0
1.17	29.71	1.43	36.32	29.2	130	36.4	162	40.2	44.2
.54	13.72	.71	18.03	33.3	148	49.8	222	38.5	42.3
1.51	38.35	1.65	41.91	24.0	107	39.0	173	47.6	52.3
2.25	57.15	2.73	69.34	12.3	54	24.3	108	41.0	45.0
2.47	62.74	2.81	71.37	14.0	62	22.8	101	39.0	42.9
1.78	45.21	2.13	54.10	14.8	66	27.1	121	39.0	42.9
.70	17.78	.93	23.62	----	---	47.1	210	43.4	47.7
.53	13.46	.78	19.81	29.4	131	48.4	215	40.3	44.3
1.07	27.18	1.20	30.48	30.0	133	39.0	173	48.2	52.9
1.12	28.44	1.37	34.80	30.0	133	36.0	160	39.4	43.3
.55	13.97	.72	18.29	----	---	47.5	211	37.6	41.3

(b) 2024-T3 alloy

a_i		a_f		P_i	P_f		k_c	
in.	mm	in.	mm	(a)	kips	kN	ksi-in$^{1/2}$	MN/m$^{3/2}$
1.98	50.3	2.82	71.6		32.0	142	55.9	61.4
2.70	68.6	3.24	82.3		26.8	119	52.8	58.0
2.58	65.5	3.28	83.3		28.2	125	55.8	61.3
2.45	62.2	3.30	83.8		29.5	131	56.9	62.5
2.43	61.7	3.06	77.7		30.0	133	55.8	61.3
1.56	39.6	2.42	61.5		36.8	164	58.0	63.7
1.83	46.5	2.72	69.1		34.7	154	59.0	64.8
2.25	57.2	2.88	73.2		31.7	141	56.3	61.9
2.23	56.6	3.24	82.3		29.8	133	58.7	64.5
1.57	39.9	2.32	58.9		36.8	164	54.8	60.2
1.80	45.7	2.58	65.5		34.2	152	55.5	61.0
1.52	38.6	2.38	60.5		37.5	167	58.7	64.5
2.02	51.3	2.48	63.0		34.4	153	54.9	60.3
1.58	40.1	2.28	57.9		39.7	177	57.5	63.2
2.56	65.0	3.22	81.8		27.7	123	54.1	59.5
1.52	38.6	2.32	58.9		38.0	169	57.8	63.5
1.50	38.1	2.38	60.5		37.0	165	59.0	64.8

[a]Could not be determined from film.

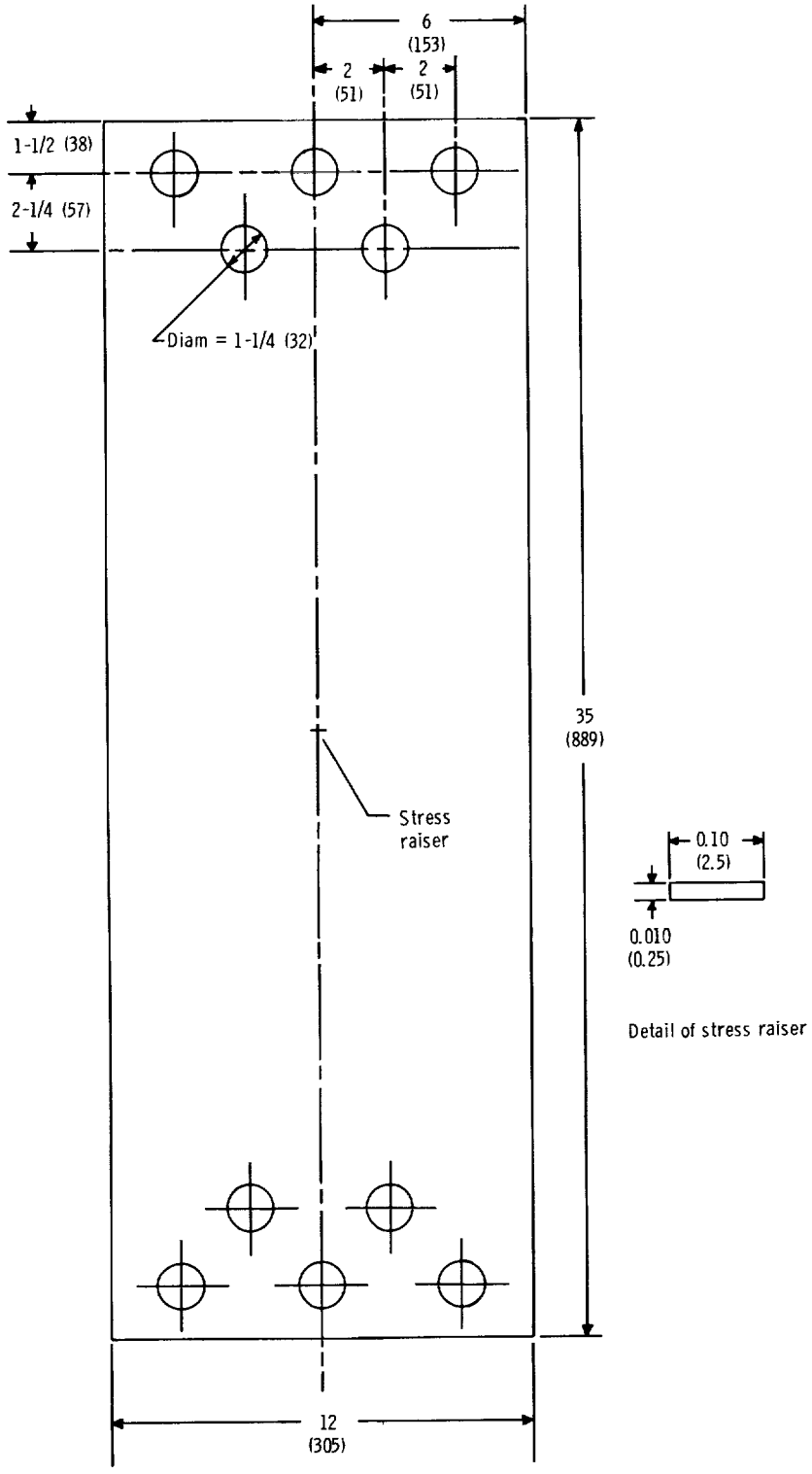

Figure 1.- Specimen configuration. (All dimensions are given first in inches and parenthetically in mm.)

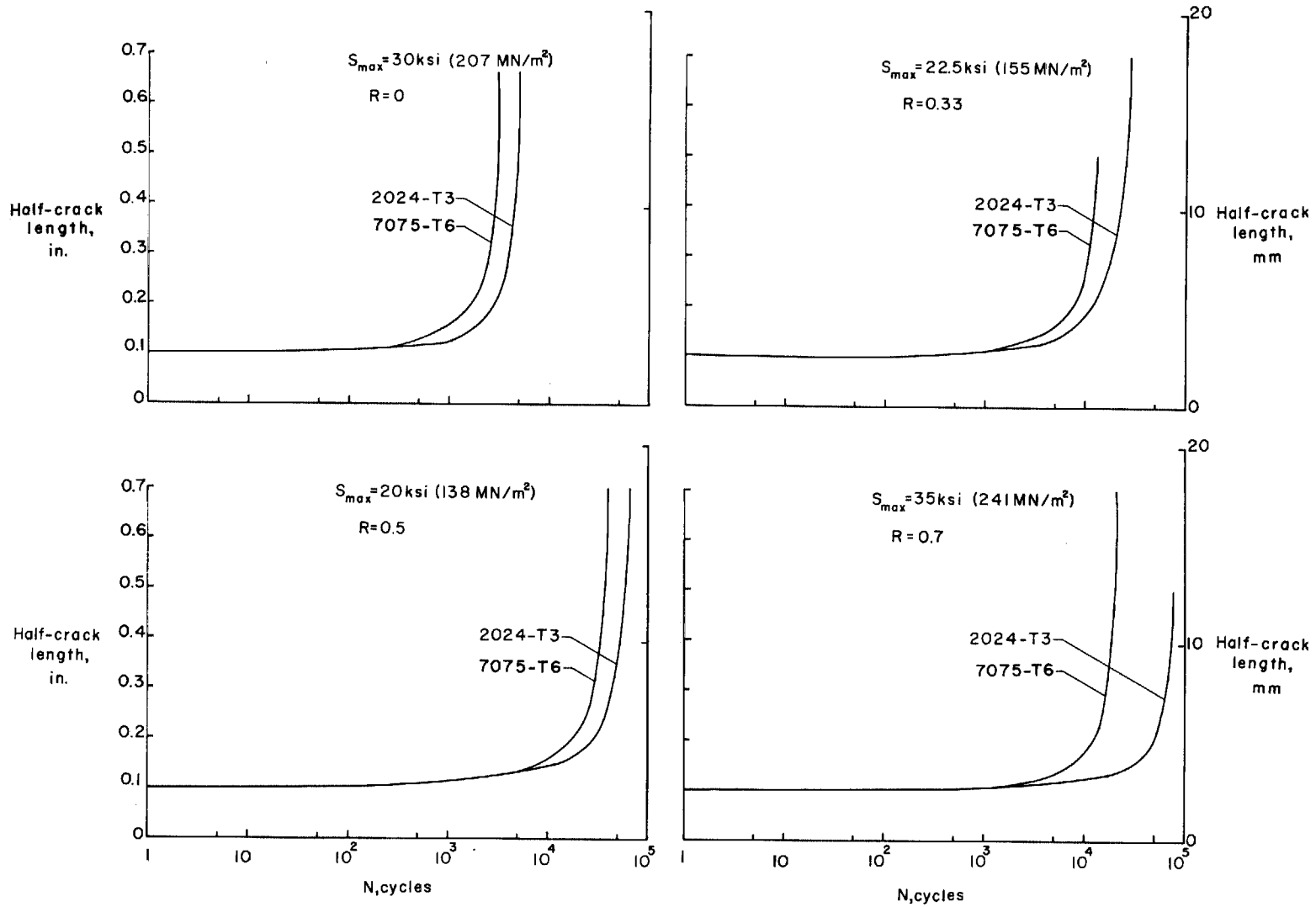

Figure 2.- Fatigue-crack-growth curves for 7075-T6 and 2024-T3 specimens tested under identical loading conditions.

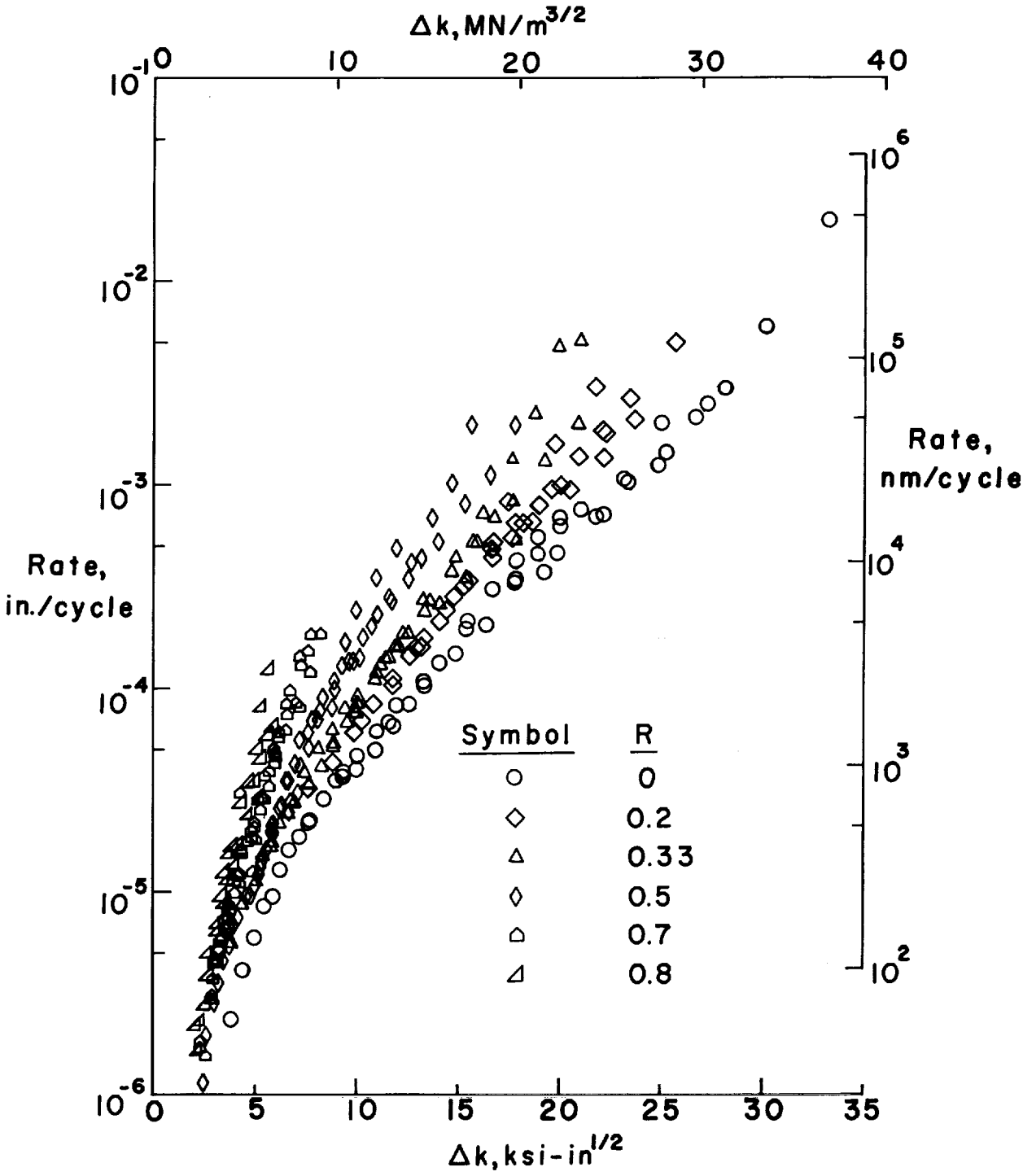

(a) 7075-T6 alloy.

Figure 3.- Variation of fatigue-crack-growth rate with Δk for $R \geq 0$.

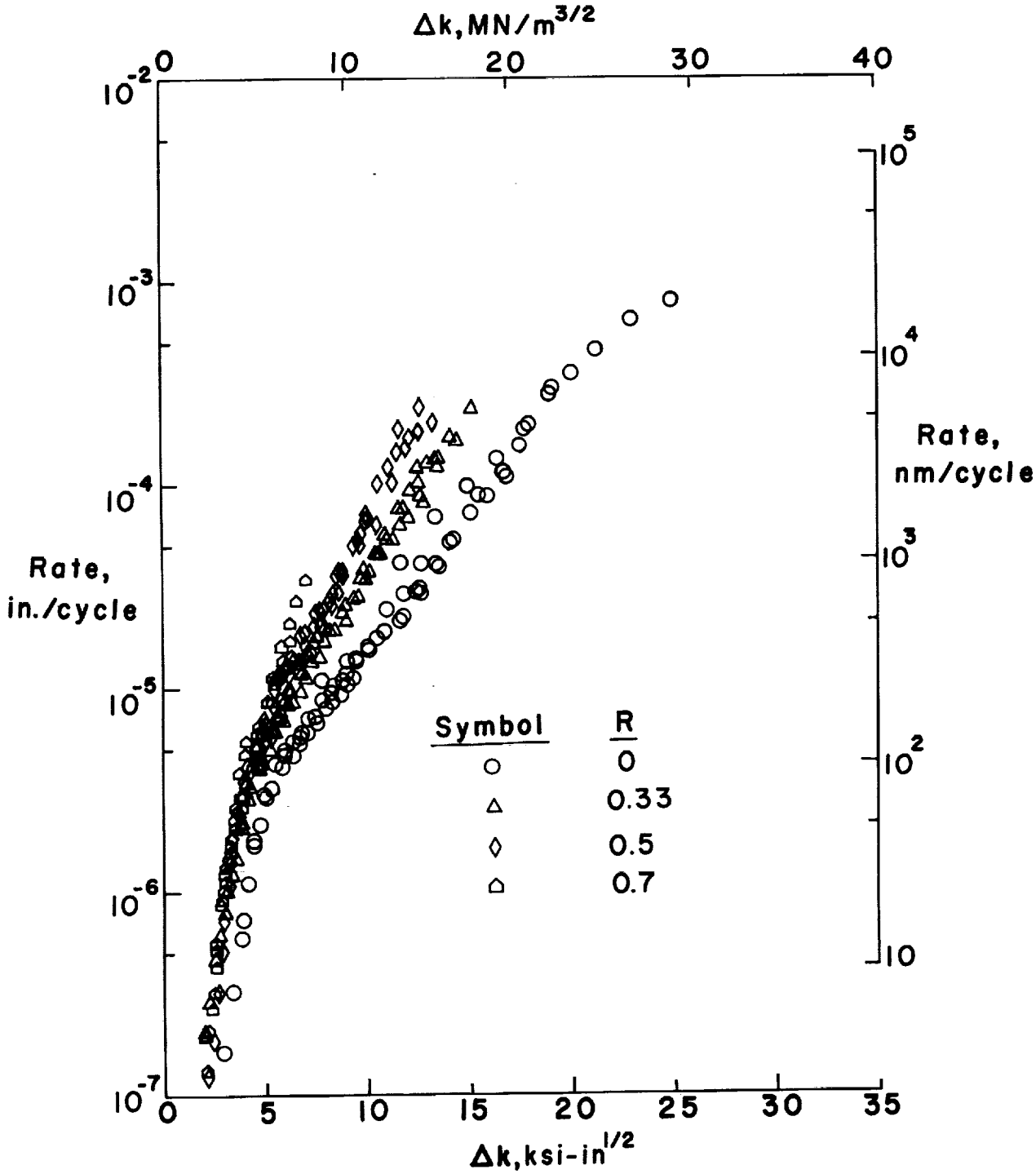

(b) 2024-T3 alloy.

Figure 3.- Concluded.

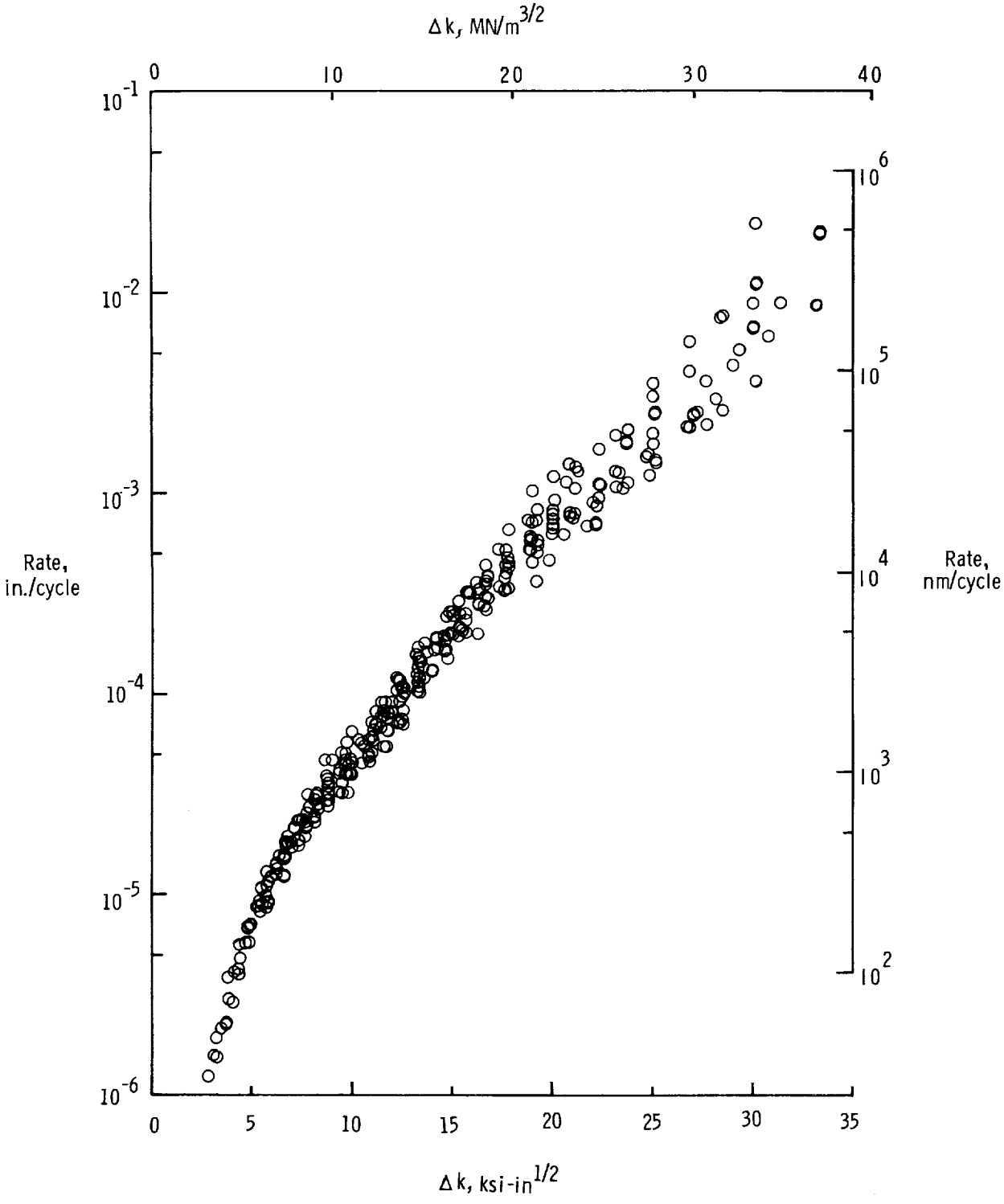

Figure 4.- Variation of fatigue-crack-growth rate with Δk for $R < 0$ in 7075-T6 alloy.

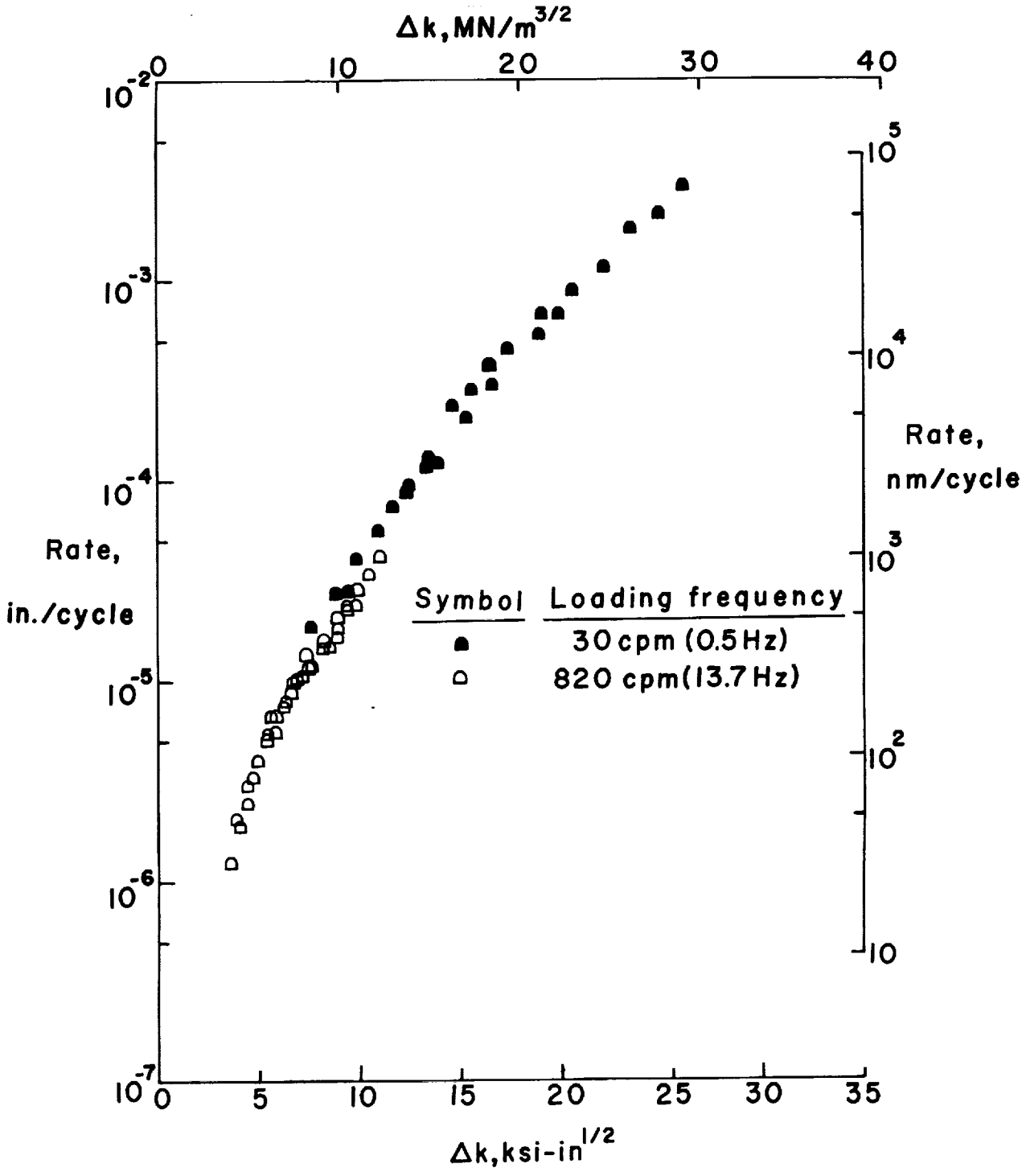

Figure 5.- Variation of fatigue-crack-growth rate with Δk for R = -1 in 2024-T3 alloy. (Data are for two loading frequencies.)

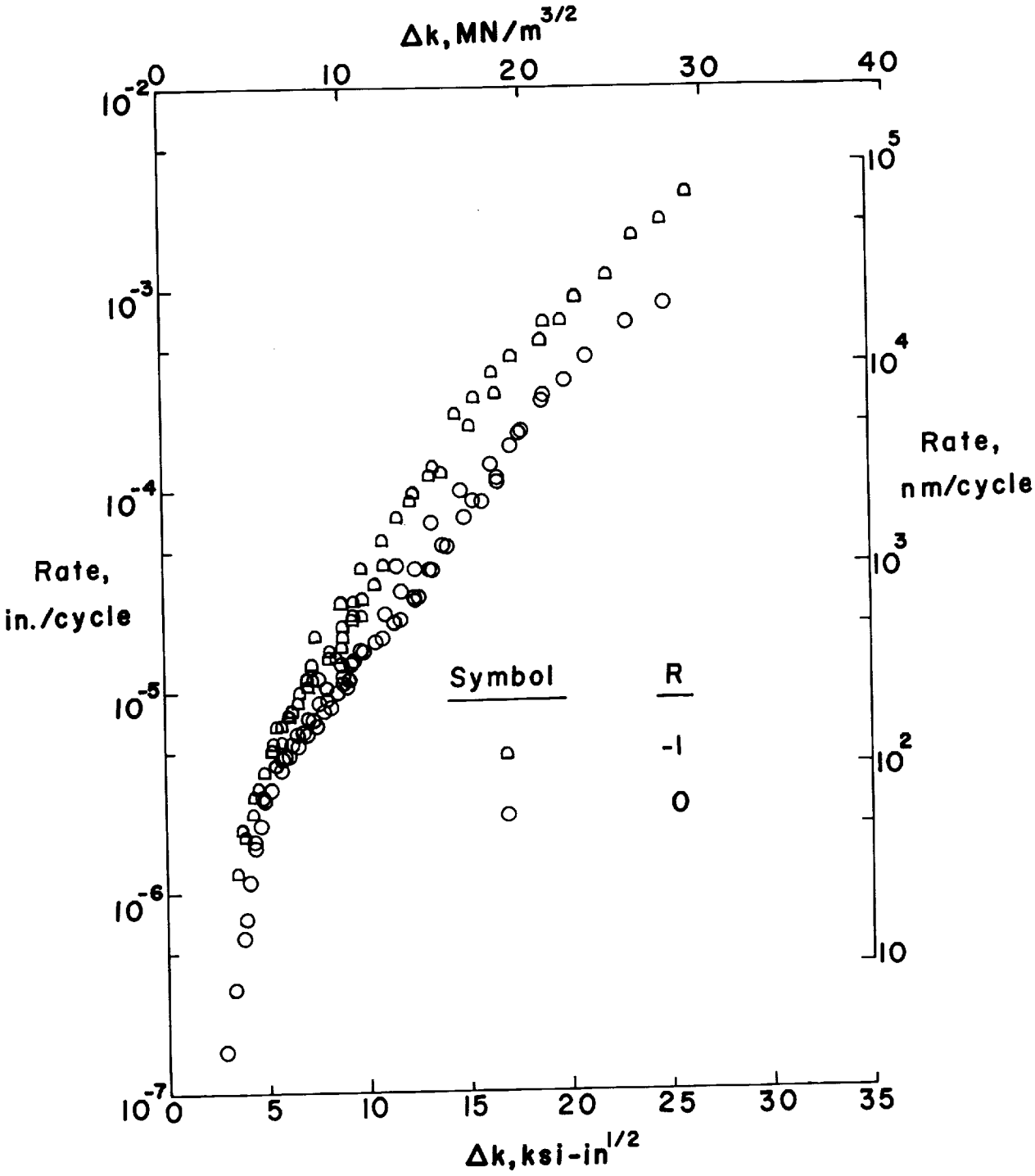

Figure 6.- Variation of fatigue-crack-growth rate with Δk for R = 0 and R = -1 in 2024-T3 alloy.

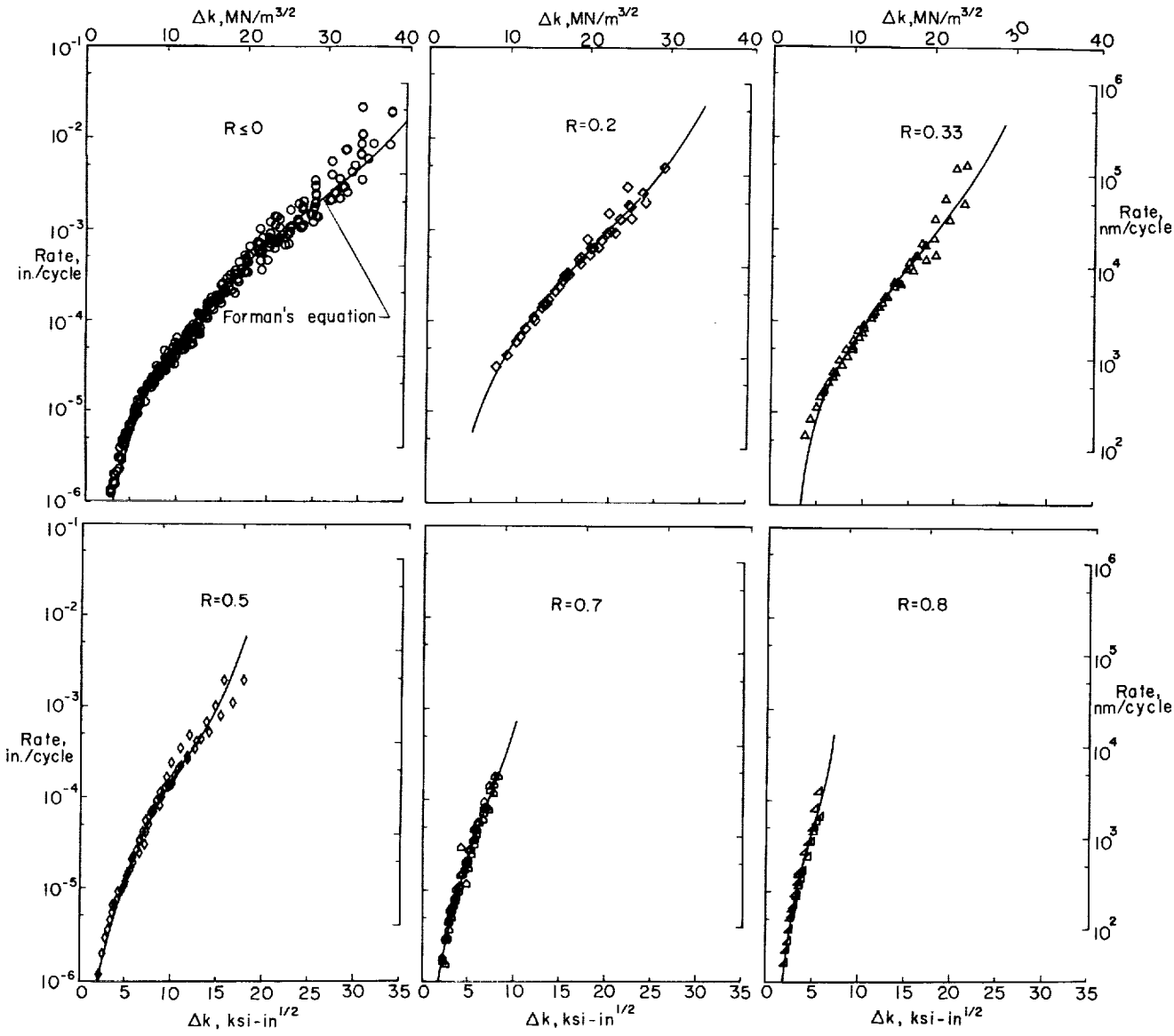

(a) 7075-T6 alloy.

Figure 7.- Correlation of experimental fatigue-crack-growth rates at various stress ratios with Forman's equation (ref. 2).

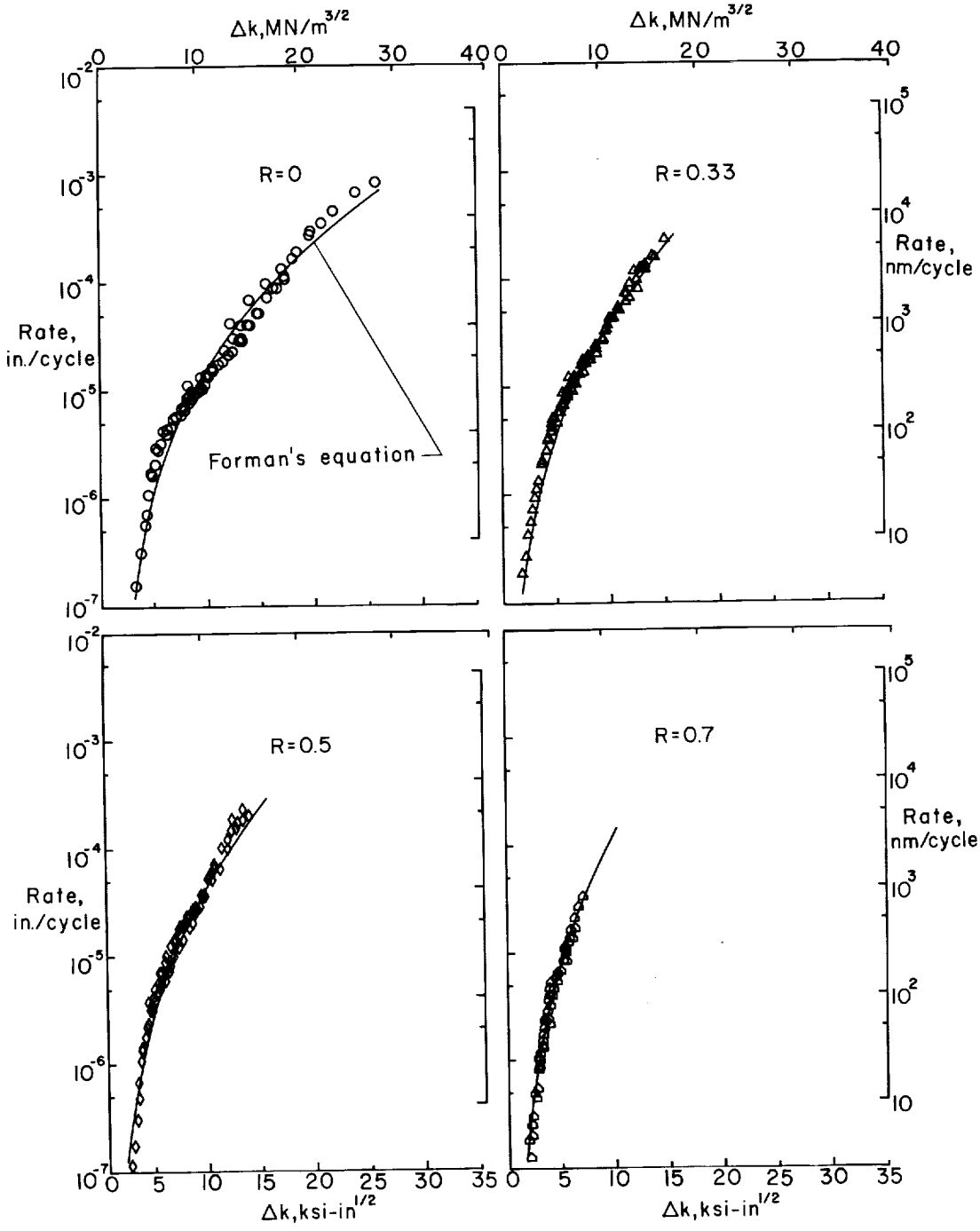

(b) 2024-T3 alloy.

Figure 7.- Concluded.

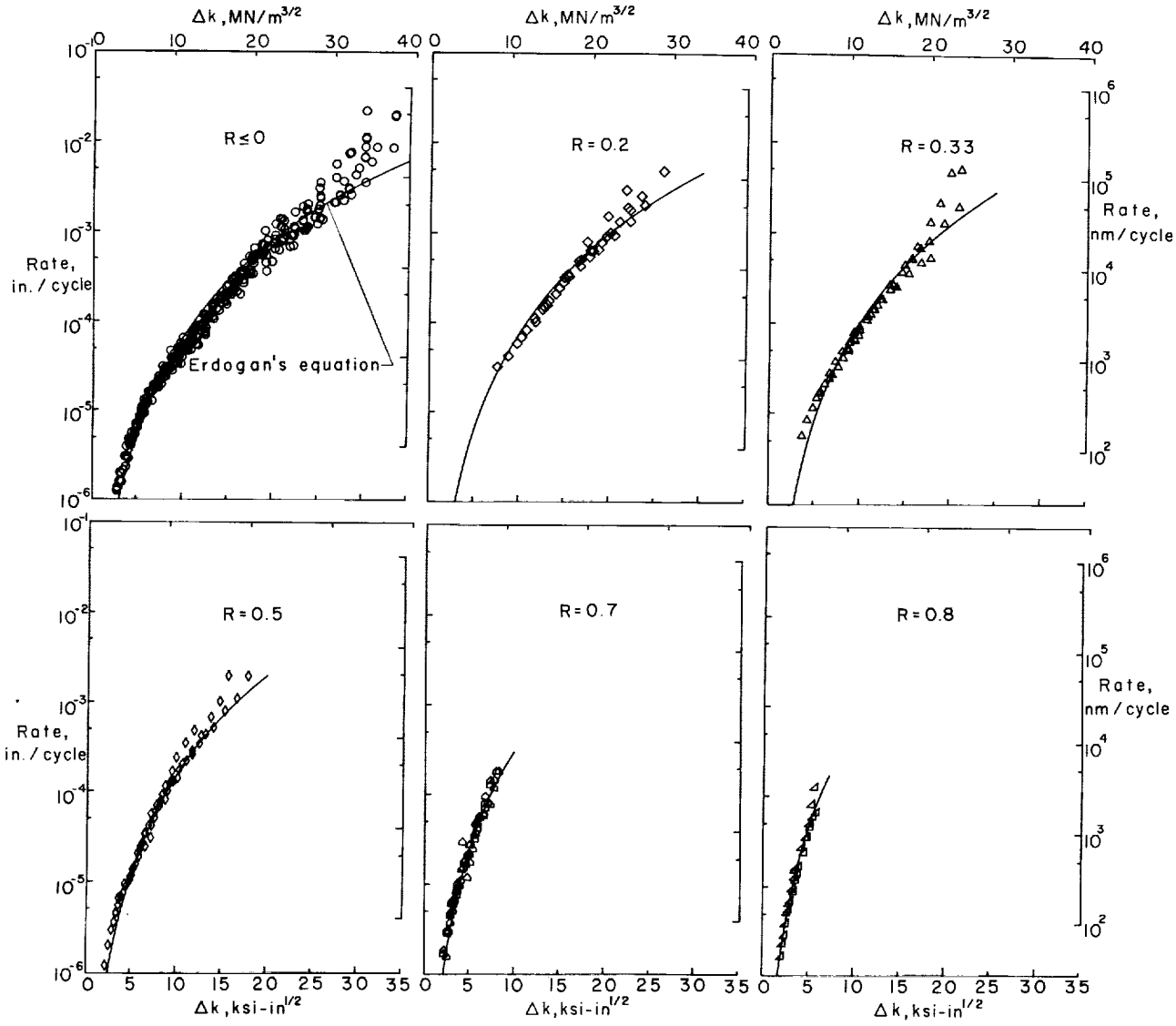

(a) 7075-T6 alloy.

Figure 8.- Correlation of experimental fatigue-crack-growth rates at various stress ratios with Erdogan's equation (ref. 3).

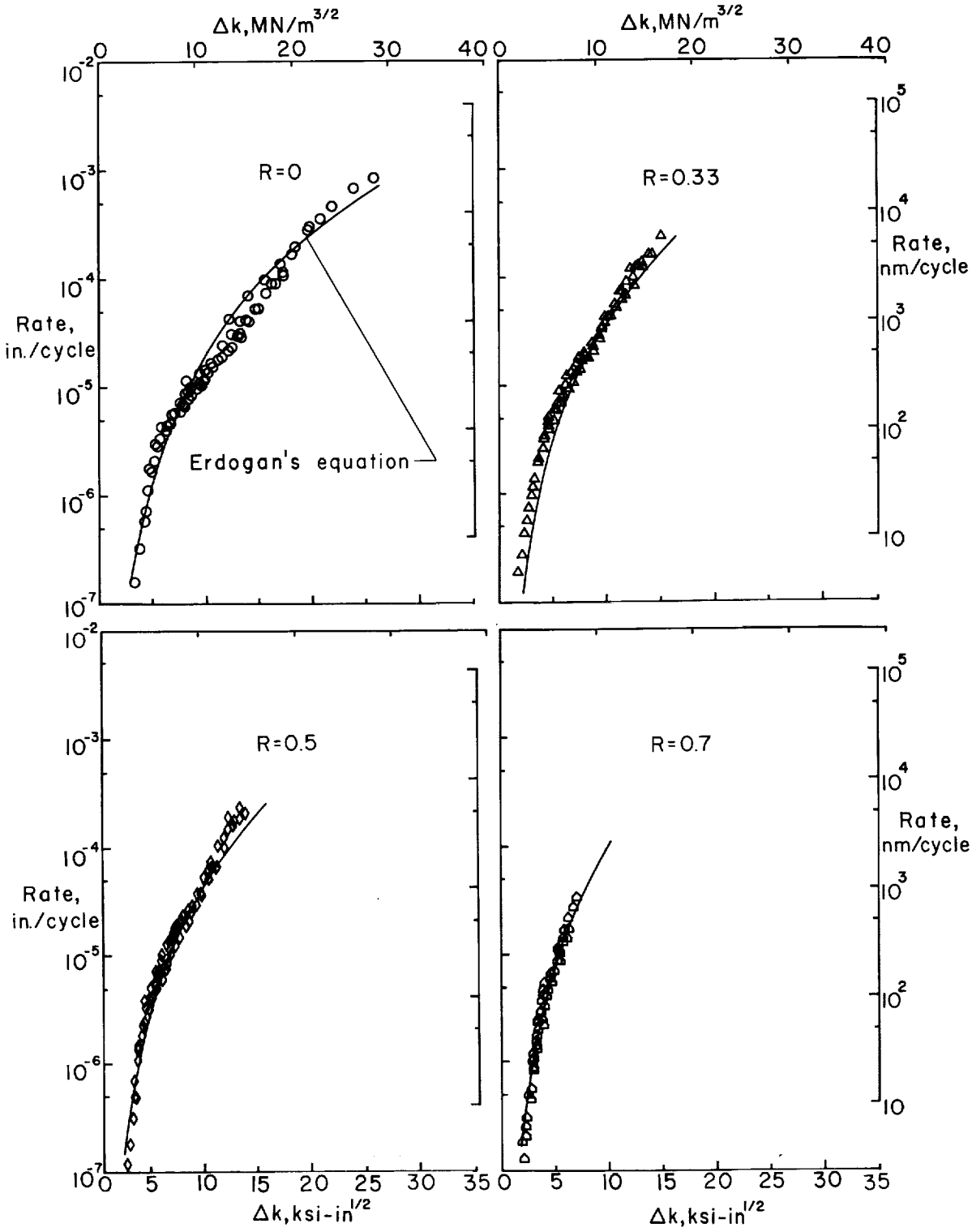

(b) 2024-T3 alloy.

Figure 8.- Concluded.

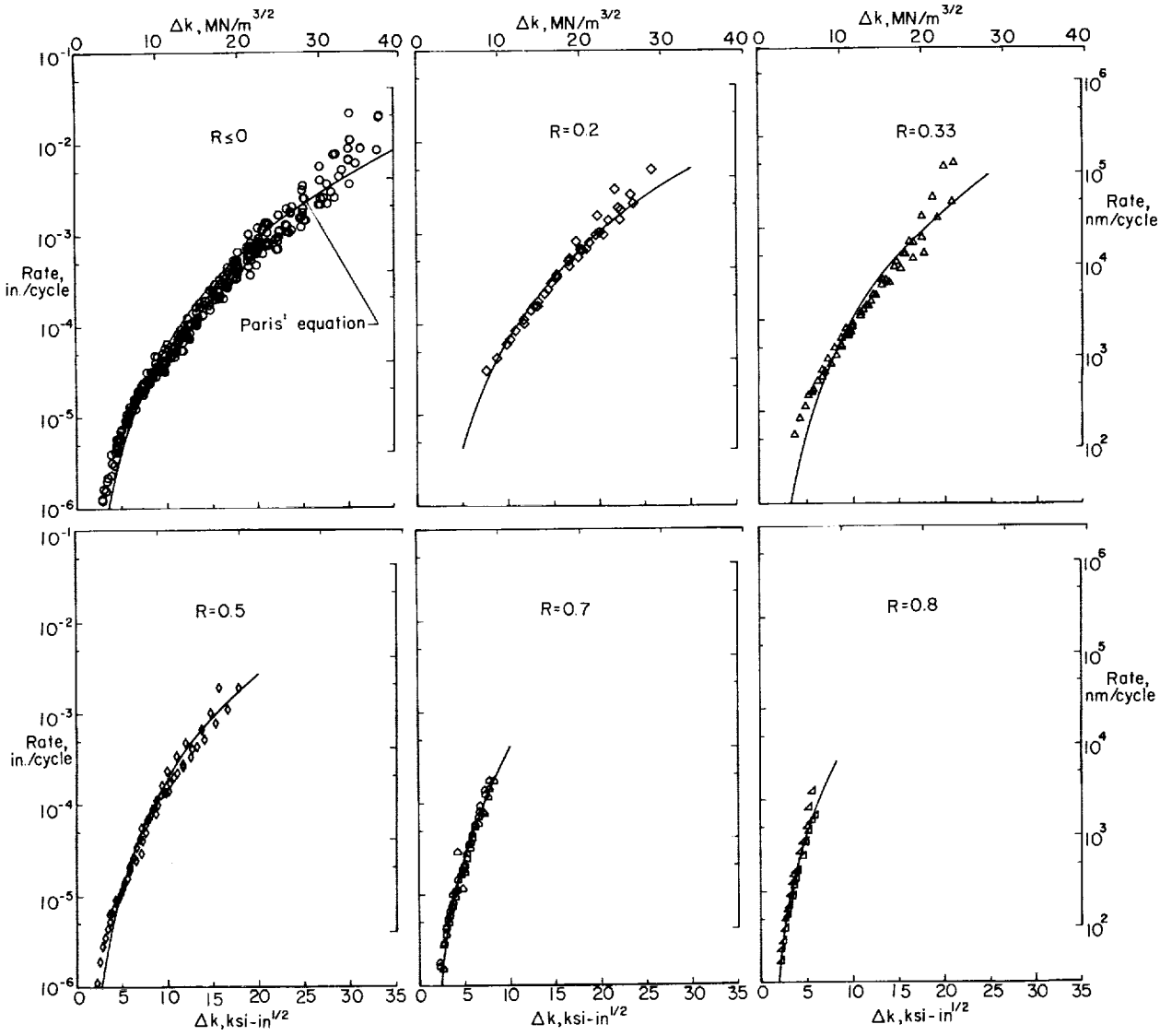

(a) 7075-T6 alloy.

Figure 9.- Correlation of experimental fatigue-crack-growth rates at various stress ratios with Paris' equation (ref. 4).

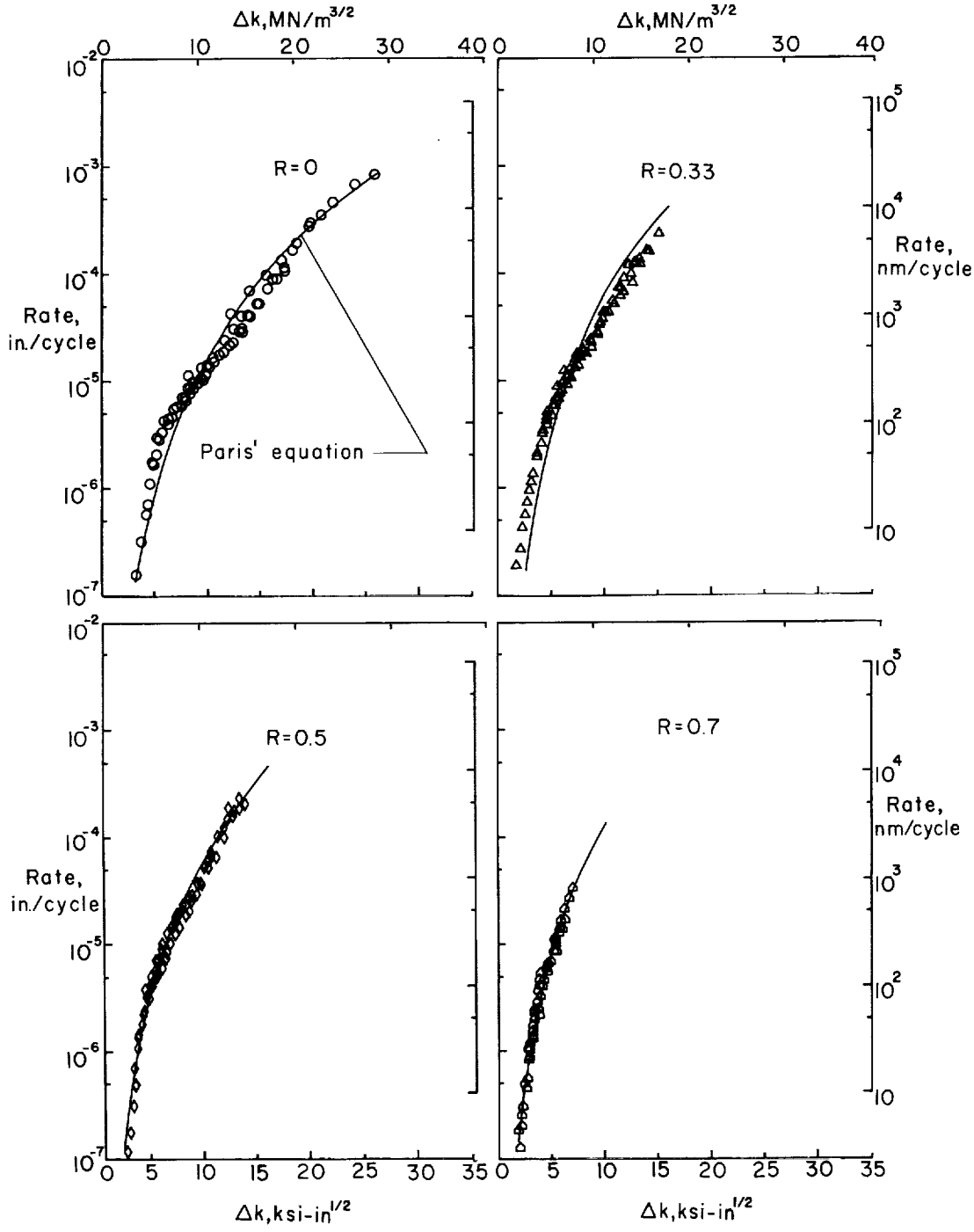

(b) 2024-T3 alloy.

Figure 9.- Concluded.